Korean J. Chem. Eng., 32(11), 2347-2354 (2015)
DOI: 10.1007/s11814-015-0044-8

pISSN: 0256-1115
eISSN: 1975-7220

Cassava starch graft copolymer as an eco-friendly corrosion inhibitor for steel in H_2SO_4 solution

Xianghong Li*,† and Shuduan Deng**

*Faculty of Science, Southwest Forestry University, Kunming 650224, P. R. China
**Yunnan Key Laboratory of Wood Adhesives and Glue Products, Southwest Forestry University, Kunming 650224, P. R. China

(*Received 31 October 2014 • accepted 25 February 2015*)

Abstract−Cassava starch graft copolymer (CSGC) was prepared by grafting acryl amide (AA) onto cassava starch (CS). The inhibition effect of CSGC on the corrosion of cold rolled steel (CRS) in 1.0 M H_2SO_4 solution was first studied by weight loss, potentiodynamic polarization curves, electrochemical impedance spectroscopy (EIS) and scanning electron microscope (SEM) methods. The results show that CSGC is a good inhibitor, and inhibition efficiency of CSGC is higher than that of CS or AA. The adsorption of CSGC on steel surface obeys Langmuir adsorption isotherm. CSGC is a mixed-type inhibitor at 20 °C, while mainly a cathodic inhibitor at 50 °C.

Keywords: Corrosion Inhibitor, Sulfuric Acid, Steel, Graft Copolymer, Adsorption

INTRODUCTION

Using inhibitors is one of the most practical methods for protecting metals against corrosion, especially in acid media [1]. Polymer inhibitors are considered to be the hot topic as the adsorption film of polymer on metal surface is thicker than that of low molecular inhibitor [2]. Up to now, some petrochemical polymers have been reported as good corrosion inhibitors for steel in acid solutions (HCl, H_2SO_4, H_3PO_4, HNO_3, etc.), such as polyvinylpyrrolidone (PVP) [3], polyethylene glycol (PEG) [4], polyoxyethylene sorbitan trioleate (tween-85) [5], quaternary polyethyleneimine (QPEI) [6], 1,6-hexanediamine-based N,N-diallyl quaternary ammonium salt polymer (HDBDQASP) [7], polyaniline (PA) [8], poly (p-phenylene diamine) (PPDA) [9], polyaspartic acid (PASP) [10], octyl-phenol-polyoxyethylene ether phosphate (OPP) [11], polyacrylic acid (PAA) [12], poly (2-acrylamino-2-methylpropane sulfonic acid) (PAMPS) [13] and polyethoxylated maleopimaric acid glycerol ester (MRGEO) [14]. However, these petrochemical polymers have some limitations such as narrow source, complex synthesis pathway, low water solubility and high cost. Owing to the increasing shortage of petrochemical raw materials, the application and development prospect of these synthesized petrochemical polymers are more severely constrained.

Natural polymer, however, is low-cost, wide source, environmentally safe and capable of biological degradation, so natural polymer could be deemed as a corrosion inhibitor with good prospects, due to both economic and environmental benefits. The natural polymers of starch [15] and chitosan [16] have been used as corrosion inhibitors of steel in acidic media. However, the inhibitive performance of natural polymer is always lower than that of petrochemical polymer. Thus, it is necessary to chemically modify the natural polymer to improve the inhibition efficiency. Previously, some chemically modified natural polymers like oxidized phosphated starch (OPS) [17], modified lignosulfonate GCL2-D1 [18] and modified vegetable gelatin [19] have been reported as effective inhibitors for steel. Through these studies, the modified natural polymers exhibit higher inhibitive performance than un-modified natural polymers.

For our research group, much work has been conducted to study the corrosion inhibition of metals by the chemically modified natural polymer of cassava starch graft copolymer (CSGC). The main chosen reason for the raw material of cassava starch is that the annual production capacity of cassava starch is higher than a million tons in the world. Recently, CSGC has been reported as a good inhibitor for steel in HCl solution [20]. The good inhibitive performance of GSGC in HCl solution promotes further study of GSCS in H_2SO_4 solution. In the present work, CSGC was prepared by grafting acryl amide onto cassava starch with oxidization reduction reaction. The inhibition effect of CSGC on the corrosion of cold rolled steel (CRS) in 1.0 M H_2SO_4 solution was studied by weight loss, potentiodynamic polarization curves and electrochemical impedance spectroscopy (EIS) and scanning electron microscope (SEM) methods. The adsorption isotherm of CSGC on steel surface was obtained. Thermodynamic parameters (standard adsorption enthalpy ΔH^0, standard adsorption free energy ΔG^0 and standard adsorption entropy ΔS^0) were calculated and discussed in detail. The inhibitive mechanism is proposed from the viewpoint of adsorption theory. It is expected to obtain general information on the inhibition effect of CSGC on steel in H_2SO_4 solution.

EXPERIMENTAL

1. Materials

Tests were performed on a cold rolled steel (CRS) of the follow-

†To whom correspondence should be addressed.
E-mail: xianghong-li@163.com

ing composition: 0.07% C, 0.3% Mn, 0.022% P, 0.010% S, 0.01% Si, 0.030% Al, and bal. Fe. Aggressive solutions of 1.0 M H_2SO_4 were prepared by dilution of AR grade 98% H_2SO_4 with distilled water.

Cassava starch graft copolymer (CSGC) was synthesized in our laboratory according to the following procedure [21]. Initially, 5 g cassava starch (CS) was placed in 250 ml three necked flask, then poured to 100 ml distilled water. Then CS water solution was heated to 80 °C for 0.5 h with continuous stirring and bubbling N_2 to remove O_2. After CS was completely gelatinized, the reaction system was cooled to 40 °C. Subsequently, 7.5 g acrylamide (AA) was added and stirred at 40 °C for 10 min, then 30 ml 0.01 M $(NH_4)_2S_2O_8$ was added, and 30 ml 0.01 M NH_4HSO_3 was slowly dropped. These mixtures were stirred at 40 °C for 3.5 h, and cooled at room temperature. Thereafter, the mixtures were poured into 350 ml absolute C_2H_5OH, then white product was fully precipitated at the bottom of beaker. Through a filter, the white precipitate was obtained, and then dried in vacuum drying oven at 50 °C for 24 h. The dried white solid product was refluxed for about 10 h using acetone; then the refluxed solution was again filtered and solid product was obtained. The product was again dried in vacuum drying oven at 50 °C for 24 h. Lastly, about 11 g white solid cassava starch graft copolymer (CSGC) was obtained for complete dryness, and preserved in a desiccator. The spectra of CSGC including Fourier transform infrared spectroscopy (FTIR), ultraviolet and visible spectrophotometry (UV-vis) and Raman spectroscopy (RS) were fully studied in our recent paper [21]. The molecular structure of CSGC is shown in Fig. 1, where AGU is starch glucose ring unit, and AA is monomer of acrylamide.

2. Weight Loss Measurements

The CRS rectangular coupons of 2.5 cm×2.0 cm×0.06 cm were abraded by a series of emery paper (grade 320-500-800) and then washed with distilled water, degreased with acetone, and finally dried at room temperature. After weighing using digital balance with sensitivity of ±0.1 mg, the specimens were totally immersed in glass beakers containing 250 ml 1.0 M H_2SO_4 without and with different inhibitor concentrations using glass hooks and rods. The temperature (±0.1 °C) was controlled at a certain value using the water thermostat bath. All the aggressive acid solutions were open to air without bubbling. After 6 h, the specimens were taken out, washed with bristle brush under running water to remove the corrosion product, dried with a hot air stream, and re-weighed accurately. For good reproducibility, experiments were done in duplicate. The average weight loss of two parallel CRS sheets was obtained, and then the inhibition efficiency (η_w) was calculated [22]. The relative phase difference (RPD) for two parallel percentage inhibition efficiency is less than 5%, which confirms the reproducibility was very precise.

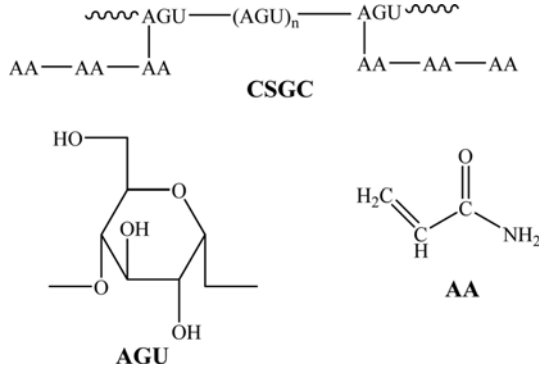

Fig. 1. The molecular structure of CSGC.

3. Electrochemical Measurements

Electrochemical experiments were carried out in the conventional three-electrode system with a platinum counter electrode (CE), a saturated calomel electrode (SCE) coupled to a fine Luggin capillary as the reference electrode and working electrode (WE). WE was in the form of a square CRS embedded in polyvinyl chloride (PVC) holder using epoxy resin so that the flat surface was the only surface in the electrode. The working surface area was 1.0 cm× 1.0 cm, and prepared as described above (Section 2.2). The electrode was immersed in test solution at open circuit potential (OCP) for 2 h to be sufficient to attain a stable state before measurement. To minimize ohmic contribution, the Luggin capillary was placed close to WE. All electrochemical measurements were at 20 °C using PARSTAT 2273 advanced electrochemical system (Princeton Applied Research). For the electrochemical measurements, each experiment was repeated at least three times to check the reproducibility.

The potentiodynamic polarization curves were carried out by polarizing to ±250 mV with respect to open circuit potential (OCP) at a scan rate of 0.5 mV s^{-1}. Inhibition efficiency (η_p) was calculated through the corrosion current density (i_{corr}) values [22]. Electrochemical impedance spectroscopy (EIS) was at OCP over a frequency range of 100 kHz-10 mHz using a 10 mV r.m.s. voltage excitation. The total number of points was 30. Inhibition efficiency (η_R) was estimated by using the charge transfer resistance (R_t) values [22].

4. Scanning Electron Microscope (SEM)

Samples of dimension 2.5 cm×2.0 cm×0.06 cm were prepared as described above (Section 2.2). After immersion in 1.0 M H_2SO_4 without and with 100 mg l^{-1} CSGC at 20 °C and 50 °C for 6 h, the specimens were cleaned with distilled water, dried with a cold air blaster, and then immediately examined using S-3000N scanning electron microscope (Hitachi High-Tech Science Systems Corporation, Japan).

RESULTS AND DISCUSSION

1. Weight Loss Measurements

1-1. Effect of CSGC on Inhibition Efficiency

Fig. 2 shows the inhibition efficiency (η_w) values obtained from the weight loss for different CSGC concentrations in 1.0 M H_2SO_4 at 20-50 °C. When the concentration of CSGC is lower than 50 mg l^{-1}, η_w increases sharply with an increase in concentration, while a further increase causes no appreciable change in performance. This behavior is due to the fact that the adsorption coverage of inhibitor on CRS surface increases with the inhibitor concentration. Along with the increase of inhibitor concentration, the adsorption amount gradually reaches saturated state, and so the inhibition performance changes slightly within the concentrations from 50 to 100 mg l^{-1}. The maximum η_w of 100 mg l^{-1} is 92.4% (RPD=2.2%) at 20 °C; 93.6% (RPD=1.8%) at 30 °C; 91.4% (RPD=2.9%) at 40 °C; and 90.3% (RPD=3.5%) at 50 °C. This result indicates that CSGC acts as a

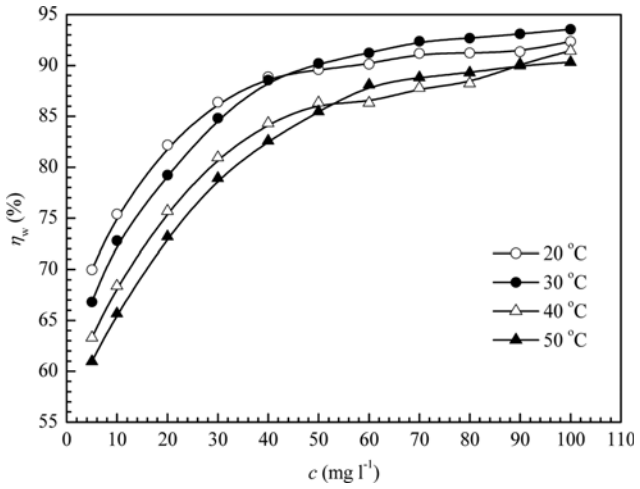

Fig. 2. Relationship between inhibition efficiency (η_w) and concentration of CSGC (c) in 1.0 M H_2SO_4.

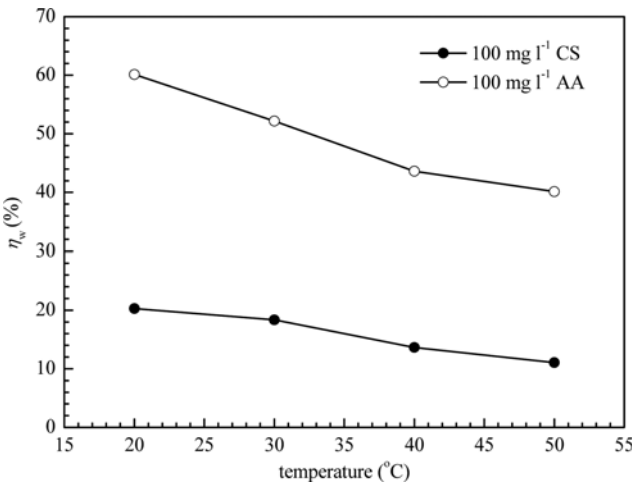

Fig. 3. Relationship between inhibition efficiency (η_w) of individual 100 mg l^{-1} CS or 100 mg l^{-1} AA and temperature in 1.0 M H_2SO_4.

good inhibitor for CRS in 1.0 M H_2SO_4.

To determine whether grafting AA onto CS is necessary, additional experiments of the inhibition effect of individual AA and CS in 1.0 M H_2SO_4 solution were done. Fig. 3 shows the inhibition efficiency (η_w) values of 100 mg l^{-1} AA and 100 mg l^{-1} CS in 1.0 M H_2SO_4 solution at 20-50 °C. Clearly, the natural polymer of CS has a negligible effect, and η_w values at all temperatures are lower than 20%. For the monomer of AA, η_w values at all temperatures are in the range from 40% to 60%. In summary, CS exhibits almost no inhibitive ability on steel in 1.0 M H_2SO_4, and AA exhibits moderate inhibitive ability, but CSGC behaves as a good inhibitor. Therefore, it could be reasonably deduced that CSGC acts as an efficient corrosion inhibitor owing to the grafting AA onto CS. The better inhibitive performance of CSGC than either AA or CS could be explained as follows: CSGC contains both N and O atoms with plentiful lone electrons, which could be responsible for the adsorption mechanism on the steel surface. CSGC has the combined advantage of CS and AA. The grafting monomer of AA in CSGC has additional N atoms, which favors more adsorption of CSGC, and thus improves the inhibition performance. Furthermore, the molecule covering area of CSGC is higher than that of CS or AA, and likely to efficiently cover more surface area (due to adsorption) of steel.

Fig. 2 also shows that η_w decreases with the experimental temperature at low inhibitor concentration (5-50 mg l^{-1}). On the contrary, when the inhibitor concentration is up to 50-100 mg l^{-1}, η_w fluctuates slightly with an increase in temperature. For CS and AA, inhibition efficiency decreases with an increase of temperature as shown in Fig. 3. Thus, CSGC could also exhibit good inhibitive performance at high temperature, which is a merit of inhibition action dependence on temperature.

1-2. Adsorption Isotherm

Basic information on the interaction between inhibitor and steel surface can be obtained through light on the adsorption isotherm. Attempts were made to fit experimental data with various isotherms including Frumkin, Langmuir, Temkin, Freundlich, Bockris-Swinkels and Flory-Huggins isotherms. By far the results are best fitted by Langmuir adsorption isotherm [23]:

$$\frac{c}{\theta} = \frac{1}{K} + c \quad (1)$$

where c is the concentration of inhibitor, K the adsorptive equilibrium constant and θ is the surface coverage that can be calculated by the ration of η_w%/100.

The linear regression between c/θ and c was calculated, and the

Table 1. Parameters of the linear regression between c/θ and c

Temperature (°C)	Linear correlation coefficient (r)	Slope	Intercept (mg l^{-1})	K (l g^{-1})
20	0.9999	1.06	2.5934	3.86×10^2
30	0.9998	1.04	3.5793	2.79×10^2
40	0.9995	1.07	4.3679	2.29×10^2
50	0.9997	1.06	5.0030	2.00×10^2

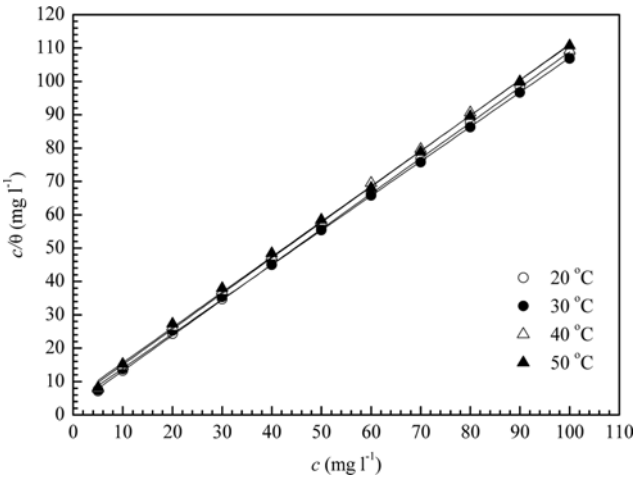

Fig. 4. Langmuir isotherm adsorption mode of CSGC on the CRS surface in 1.0 M H_2SO_4.

parameters are listed in Table 1. Fig. 4 shows the straight lines of c/θ versus c at 20-50 °C. Clearly, all linear correlation coefficients (r) and slope values are almost equal to 1, which indicates the adsorption of CSGC on steel surface obeys Langmuir adsorption isotherm. The adsorptive equilibrium constant (K) decreases with the increase of temperature, which indicates that it is easily and strongly adsorbed on the steel surface for the inhibitor at relatively lower temperature. But when the temperature is relatively high, the adsorbed inhibitor molecules tend to desorb from the steel surface.

1-3. Thermodynamic Parameters

Thermodynamic parameters are important to further understand the adsorption process of inhibitor on steel/solution interface. The standard adsorption enthalpy (ΔH^0) could be calculated on the basis of the van't Hoff equation:

$$\frac{d\ln K}{dT} = \frac{\Delta H^0}{RT^2} \quad (2)$$

where R is the gas constant (8.314 J K^{-1} mol^{-1}), T the absolute temperature, and K is the adsorptive equilibrium constant. Eq. (2) can also be changed as the following relationship [23]:

$$\ln K = \frac{-\Delta H^0}{RT} + D \quad (3)$$

where D is integration constant. Fig. 5 represents the straight lines of ln K versus 1/T with good linear relationship (the linear correlation coefficient is 0.9801). ΔH^0 is calculated from the slope ($-\Delta H^0$/R), and listed in Table 2.

The adsorptive equilibrium constant (K) is related to the standard adsorption free energy (DG0) according to [21,24,25]:

$$K = \frac{1}{c_{solvent}} \exp\left(\frac{-\Delta G^0}{RT}\right) \quad (4)$$

where $c_{solvent}$ is the concentration of water in solution. Note that the unit of $c_{solvent}$ lies in that of K. As can be seen from Table 1, the unit of K is l mg^{-1}, which results in the unit of $c_{solvent}$ being mg l^{-1} with the value of approximate 1.0×10^6 [25].

With the obtained both parameters of ΔG^0 and ΔH^0, the standard adsorption entropy (ΔS^0) can be calculated using the following thermodynamic basic equation:

$$\Delta S^0 = \frac{\Delta H^0 - \Delta G^0}{T} \quad (5)$$

All the standard thermodynamic parameters are listed in Table 2. The negative sign of ΔH^0 suggests that the adsorption of inhibitor is an exothermic process, which means that inhibition efficiency decreases with rise in the temperature. Such behavior can also be interpreted on the basis that the increase in temperature resulting in the desorption amount of some adsorbed inhibitor molecules rises with the increase of temperature from the steel surface. Generally, values of ΔG^0 up to −20 kJ mol^{-1} are consistent with the electrostatic interaction between the charged molecules and the opposite charged metal (physical adsorption), while those more negative than about −40 kJ mol^{-1} involve sharing or transfer of electrons from the inhibitor molecules to the metal surface to form a co-ordinate bond (chemisorption) [26]. Table 2 shows the values of ΔG^0 at four temperatures are within the range from –20 to –40 kJ mol^{-1}, probably meaning that both physical adsorption and chemical adsorption (mixed adsorption) would take place. Inspection of Table 2 reveals that the sign of ΔS^0 is positive. The reason could be explained as follows: The adsorption of organic inhibitor compound from the aqueous solution can be regarded as a quasi-substitution process between the organic molecules in the aqueous phase [$Org_{(sol)}$] and water molecules at the electrode surface [$H_2O_{(ads)}$] [27].

$$Org_{(sol)} + xH_2O_{(ads)} \leftrightarrow Org_{(ads)} + xH_2O_{(sol)} \quad (6)$$

where x is the size ratio, that is, the number of water molecules replaced by one organic inhibitor. In this situation, the adsorption of inhibitor is accompanied by desorption of water molecules from the surface. The thermodynamic values obtained are the algebraic sum of the adsorption of organic molecules and desorption of water molecules [28]. Therefore, the gain in entropy is attributed to the increase in solvent entropy and to more positive water desorption enthalpy [29]. The positive values of ΔS^0 also mean that an increasing in disordering takes place in reactants adsorption from inhibitor to the metal/solution interface [30], which is the driving force for the adsorption of inhibitor onto steel surface [30].

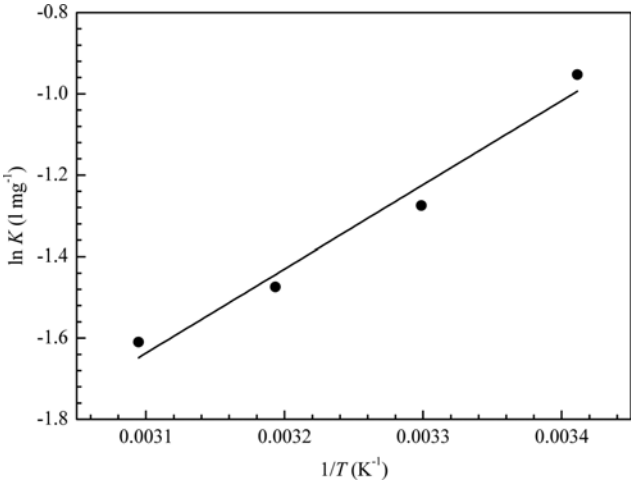

Fig. 5. The relationship between ln K and 1/T in 1.0 M H_2SO_4.

Table 2. Thermodynamic parameters of the adsorption of CSGC on CRS surface in 1.0 M H_2SO_4

Temperature (°C)	ΔG^0 (kJ mol^{-1})	ΔH^0 (kJ mol^{-1})	ΔS^0 (J mol^{-1} K^{-1})
20	−31.3	−17.2	48.1
30	−31.6	−17.2	47.5
40	−32.1	−17.2	47.6
50	−32.8	−17.2	48.2

2. Potentiodynamic Polarization Curves

Figs. 6(a) and (b) illustrate the potentiodynamic polarization curves for CRS in 1.0 M H_2SO_4 solutions without and with various concentrations of CSGC at 20 °C and 50 °C, respectively. At 20 °C, the presence of CSGC causes a remarkable decrease in the corrosion rate, i.e., shifts both anodic and cathodic curves to lower values of corrosion current densities. Namely, both cathodic and anodic reactions of CRS electrode corrosion are drastically retarded

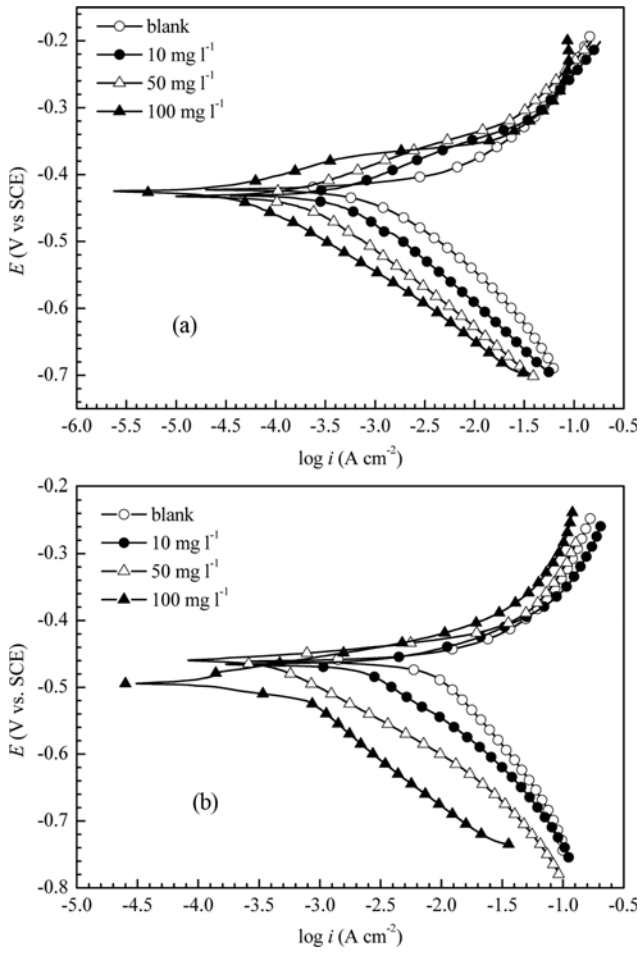

Fig. 6. Potentiodynamic polarization curves for CRS in 1.0 M H_2SO_4 without and with different concentrations of CSGC (immersion time is 2 h): (a) 20 °C; (b) 50 °C.

by CSGC. On the other hand, the anodic reaction of the corrosion process is slightly inhibited at 50 °C. This means that CSGC acts as a mixed-type inhibitor at 20 °C, while mainly behaves as a cathodic inhibitor at 50 °C.

Electrochemical parameters of corrosion current densities (i_{corr}), corrosion potential (E_{corr}), cathodic Tafel slope (b_c), anodic Tafel slope (b_a) and inhibition efficiency (η_p) are presented in Table 3. Apparently, i_{corr} decreases considerably in the presence of inhibitor, and decreases with increasing the inhibitor concentration. Correspondingly, η_p increases with the increase of the inhibitor concentration, due to the increase in the blocked fraction of the electrode surface by adsorption. At 100 mg l^{-1} CSGC, the maximum η_p is up to 95.7% at 20 °C; and 93.9% at 50 °C. Compared with the electrochemical parameters at 20 °C, E_{corr} at 50 °C shifts to negative and i_{corr} to high value, which indicates the corrosion is accelerated at high temperature. At 20 °C, E_{corr} changes slightly in the presence of GSGC; therefore, it can be arranged as a mixed-type inhibitor in 1.0 M H_2SO_4, and the inhibition of GSGC on CRS is caused by geometric blocking effect [31]. Namely, the inhibition effect comes from the reduction of the reaction area on the surface of the corroding metal [31]. At 50 °C, the presence of CSGC shifts the corrosion potential to negative compared with blank solution, which indicates that CSGC mainly acts as a cathodic inhibitor [32]. But corrosion potential in the presence of inhibitors ranks the order: E_{corr} (100 mg l^{-1} CSGC)<E_{corr} (10 mg l^{-1} CSGC)<E_{corr} (50 mg l^{-1} CSGC), which indicates that there is no clear trend of corrosion potential as a function of inhibitor concentration. It can be explained that 10 mg l^{-1} CSGC has no inhibitive effect on anodic reaction, but 50 mg l^{-1} CSGC has a little inhibitive effect on anodic reaction, so the corrosion potential does not continue to shift negative. When CSGC concentration is 100 mg l^{-1}, the inhibitive effects on both anodic and cathodic reactions strengthen, but the inhibitive degree on cathodic reaction is more than that on anodic reaction, so the corrosion potential shifts more negative in the presence of 100 mg l^{-1} CSGC. Tafel slopes of b_c and b_a change upon addition of CSGC, which means that CSGC molecules are adsorbed on reactive sites, resulting in inhibiting both anodic dissolution and cathodic reduction reactions.

3. Electrochemical Impedance Spectroscopy (EIS)

Figs. 7(a) and (b) represent the Nyquist diagrams for CRS in 1.0 M H_2SO_4 in the presence of CSGC at 20 °C and 50 °C, respectively. Clearly, the impedance spectra exhibit a large capacitive loop at high frequencies followed by an inductive loop at low frequency values. At both temperatures, compared with blank solution, the shape is maintained throughout all tested concentrations, indicating that there is almost no change in the corrosion mechanism due to the inhibitor addition [33].

The capacitive loop indicates that the corrosion of steel is mainly controlled by a charge transfer process, and is usually related to the charge transfer of the corrosion process and double layer behav-

Table 3. Potentiodynamic polarization parameters for the corrosion of CRS in 1.0 M H_2SO_4 containing different concentration of CSGC at 20 °C and 50 °C

Temperature (°C)	c (mg l^{-1})	E_{corr} vs SCE (mV)	i_{corr} (μA cm^{-2})	$-b_c$ (mV dec^{-1})	b_a (mV dec^{-1})	η_p (%)
20	0	−421.0±3.4	1603.3	141	61	-
	10	−419.6±2.6	481.0	134	54	70.0
	50	−422.2±3.0	175.9	119	48	89.0
	100	−419.6±4.1	69.0	101	38	95.7
50	0	−456.2±3.5	7865.7	222	49	-
	10	−466.9±4.0	2539.7	139	42	67.7
	50	−456.2±6.8	875.9	101	21	88.9
	100	−473.0±3.3	481.8	142	32	93.9

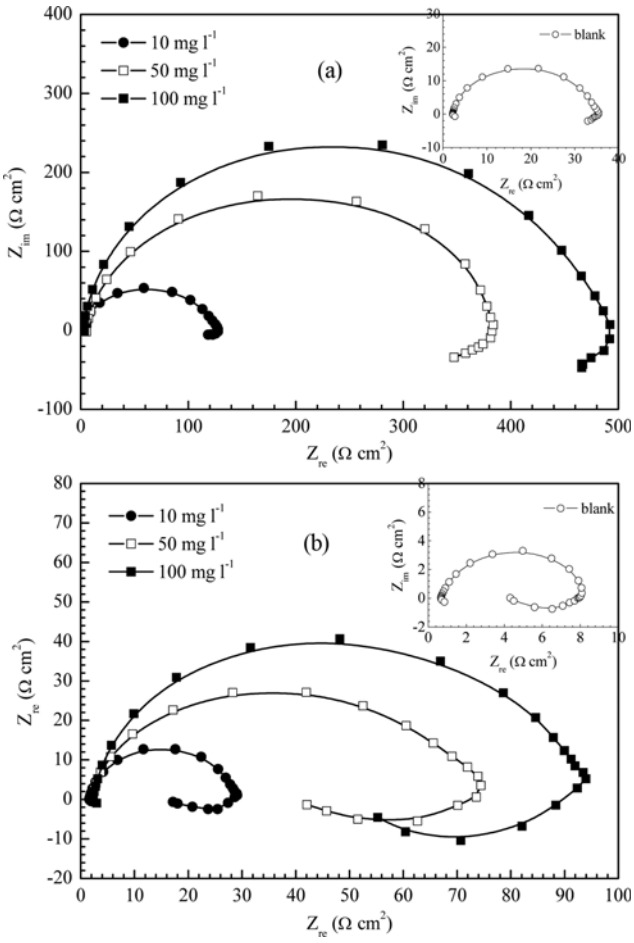

Fig. 7. Nyquist plots of the corrosion of CRS in 1.0 M H_2SO_4 without and with different concentrations of inhibitors (2 hours immersion at the open circuit potential prior to measurement): (a) 20 °C; (b) 50 °C.

ior. On the other hand, the inductive loop may be attributed to the relaxation process obtained by adsorption species like $FeSO_4$ [34] or inhibitor species [35] on the electrode surface. Noticeably, the inductive loops at 50 °C are increased to be bigger than those at 20 °C, which might be caused by more and more relaxation process at high temperature.

The diameter of the capacitive loop in the presence of CSGC is bigger than that in the absence of inhibitor (blank solution) and increases with the inhibitor concentration. This indicates that the impedance of inhibited substrate increases with the inhibitor concentration. Noticeably, these capacitive loops are not perfect semicircles, which can be attributed to the frequency dispersion effect as a result of the roughness and inhomogeneousness of the electrode surface [36]. Accordingly, the capacitive loops at high frequencies are simulated by the equivalent circuit [34] shown in Fig. 8. The circuit employed allows the identification of both solution resistance (R_s) and charge transfer resistance (R_t). Note that the double layer capacitance (C_{dl}) value is affected by imperfections of the surface, and that this effect is simulated via a constant phase element (CPE) [36]. The CPE is composed of a component Q_{dl} and a coefficient a, which quantifies different physical phenomena like

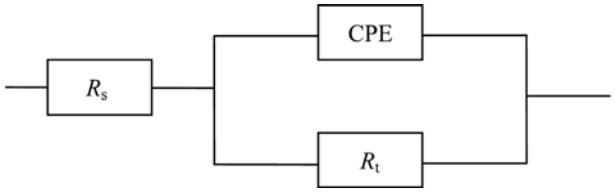

Fig. 8. The equivalent circuit model of the capacitive loop in EIS.

Table 4. EIS parameters for the corrosion of CRS in 1.0 M H_2SO_4 containing CSGC at 20 °C and 50 °C

Temperature (°C)	c (mg l^{-1})	R_s (Ω cm^2)	R_t (Ω cm^2)	a	C_{dl} (μF cm^{-2})	η_R (%)
20	0	2.29	32.3	0.9270	136	-
	10	1.97	121.5	0.9421	89	73.4
	50	4.40	374.7	0.9221	75	91.4
	100	2.68	483.1	0.9481	53	93.3
50	0	0.73	6.8	0.9349	338	-
	10	1.70	25.3	0.9468	197	73.1
	50	2.09	64.9	0.9098	118	89.5
	100	2.44	85.3	0.9281	93	92.0

surface inhomogeneousness resulting from surface roughness, inhibitor adsorption, porous layer formation, etc. The capacitance can be calculated from the following equation [37]:

$$C_{dl}=Q_{dl}\times(2\pi f_{max})^{a-1} \quad (7)$$

where f_{max} represents the frequency at which the imaginary value reaches a maximum on the Nyquist plot. The electrochemical parameters of R_s a, R_p, C_{dl} and η_R are presented in Table 4. Clearly, R_t value increases prominently while C_{dl} is reduced with the concentration of inhibitor. The greatest effect was observed at 100 mg l^{-1} of CSGC, which gives R_t value of 483.1 Ω cm^2 at 20 °C, and 85.3 Ω cm^2 at 50 °C; C_{dl} value of 53 μF cm^{-2} at 20 °C, and 93 μF cm^{-2} at 50 °C. A large charge transfer resistance is associated with a slower corroding system. On the other hand, the decrease in C_{dl} compared with that in blank solution (without inhibitor), which can result from a decrease in local dielectric constant and/or an increase in the thickness of the electrical double layer, suggests that the inhibitor molecules function by adsorption at the metal/solution interface [37]. η_R increases with the concentration of inhibitor, and follows the order: η_R (20 °C)> η_R (50 °C). The maximum η_R values are 93.3% and 92.0% at 20 °C and 50 °C, respectively. These results again confirm that CSGC exhibits good inhibitive performance for CRS in 1.0 M H_2SO_4 solution.

Inhibition efficiencies obtained from weight loss (η_w), potentiodynamic polarization curves (η_p) and EIS (η_R) are in good reasonably agreement.

4. Scanning Electron Microscope (SEM)

Fig. 9 shows the SEM photos of CRS surface in 1.0 M H_2SO_4. It can be seen from Fig. 9(a) that the CRS surface before immersion appears more uniform and some abrading scratches. Figs. 9(b) and (d) reveal that the steel surfaces after immersion in uninhibited 1.0 M H_2SO_4 at 20 °C and 50 °C appear an aggressive attack of the

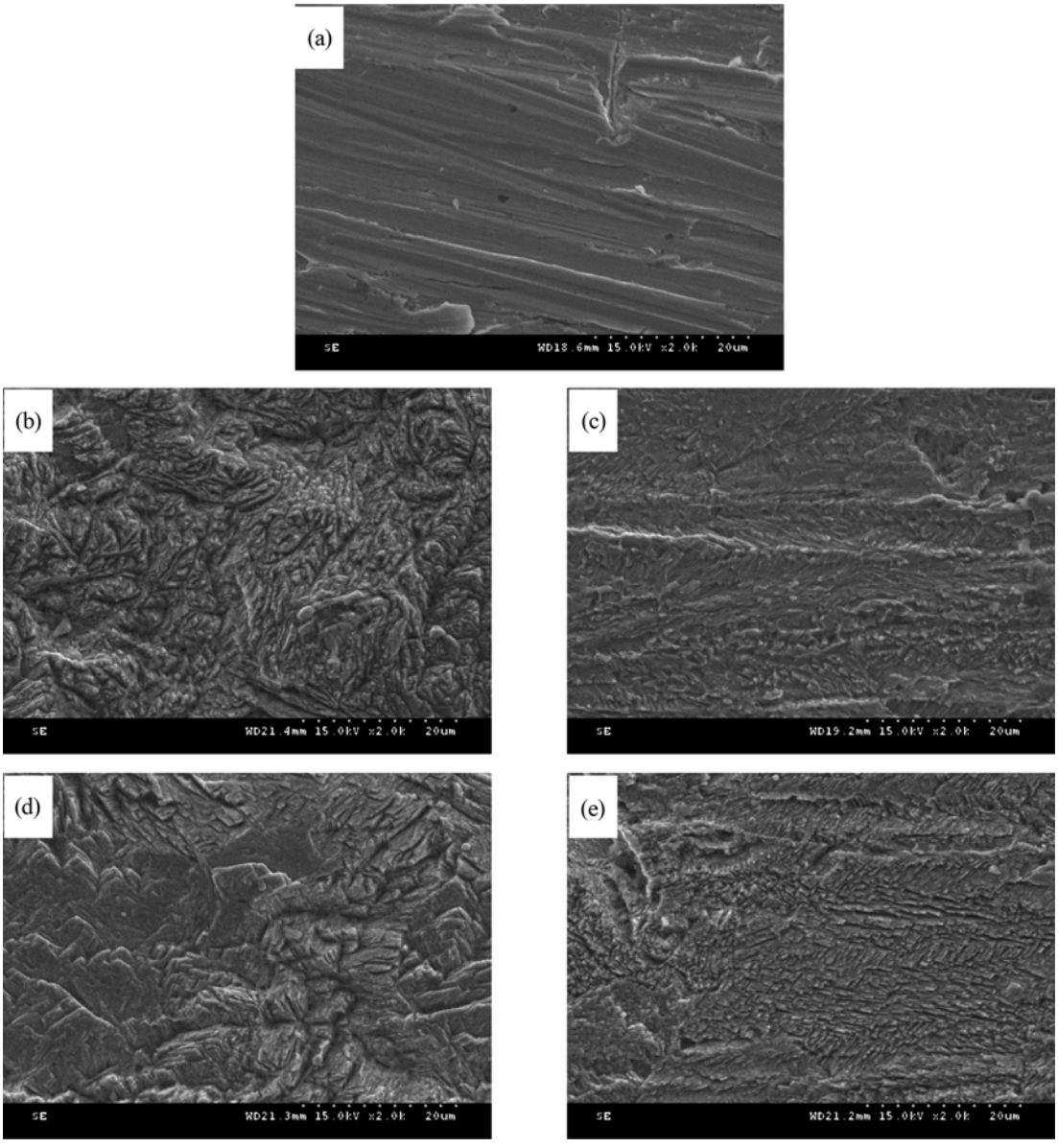

Fig. 9. SEM micrographs of CRS surface: (a) before immersion; (b) after 6 h of immersion at 20 °C in 1.0 M H_2SO_4; (c) after 6 h of immersion at 20 °C in 100 mg l^{-1} CSGC+1.0 M H_2SO_4; (d) after 6 h of immersion at 50 °C in 1.0 M H_2SO_4; (e) after 6 h of immersion at 50 °C in 100 mg l^{-1} CSGC+1.0 M H_2SO_4.

corroding medium on the steel surface. Moreover, the surface layer is rather rougher at 50 °C. In contrast, in the presence of 100 mg l^{-1} CSGC, Figs. 9(c) and (e) show that the corrosion is drastically inhibited. There is an adsorbed film adsorbed on CRS surface at either 20 °C (Fig. 9(c)) or 50 °C (Fig. 9(e)), which does not exist in corresponding Figs. 9(b) and (d). Accordingly, it could be concluded that the adsorption film can efficiently inhibit the corrosion of steel. Also, the corrosion is accelerated with the increase of temperature.

CONCLUSIONS

(1) CSGC acts as a good inhibitor for the corrosion of CRS in 1.0 M H_2SO_4. Inhibition efficiency (η_w) increases with the inhibitor concentration, and the maximum η_w of 100 mg l^{-1} is 92.4% at 20 °C; 93.6% at 30 °C; 91.4% at 40 °C; and 90.3% at 50 °C. η_w decreases with the experimental temperature.

(2) The adsorption of CSGC on CRS surface obeys the Langmuir adsorption isotherm. The adsorption is an exothermic process accompanied by an increase in entropy, and involves both physical and chemical adsorption.

(3) CSGC acts as a mixed-type inhibitor at 20 °C, while mainly the cathodic inhibitor at 50 °C. EIS spectra exhibit one capacitive loop at HF and followed by an inductive loop at LF. The inductive loops at 50 °C are larger than those at 20 °C. The addition of CSGC to 1.0 M H_2SO_4 solutions enhances R_f values while reduces C_{dl} values.

(4) SEM results confirm that the introduction of CSGC into 1.0 M H_2SO_4 solution effectively protects steel from corrosion.

ACKNOWLEDGEMENT

This work was carried out in the frame of research project supported by the Key program of Science Foundation of Educational Department of Yunnan Province (No. 2013Z080). The electrochemical measurements were made by using PARSTAT 2273 advanced electrochemical system (Princeton Applied Research) provided by Advanced Science Instrument Sharing Center of Southwest Forestry University.

REFERENCES

1. G. Trabanelli, *Corrosion*, **47**, 410 (1991).
2. X. M. Li, Y. N. Liu, J. S. Liu and C. Y. Fu, *Total Corros. Control*., **23**(2), 23 (2012).
3. Y. Jianguo, W. Lin, V. Otieno-Alego and D. P. Schweinsberg, *Corros. Sci*., **37**, 975 (1995).
4. H. Ashassi-Sorkhabi, N. Ghalebsaz-Jeddi, F. Hashemzadeh and H. Jakani, *Electrochim. Acta*, **51**, 3848 (2006).
5. X. H. Li, S. D. Deng, H. Fu and G. N. Mu, *J. Appl. Electrochem*., **39**, 1125 (2009).
6. X. Zhang, B. J. Gao and Y. L. Shen, *Chin. J. Appl. Chem*., **25**, 212 (2008).
7. S. A. Ali and M. T. Saeed, *Polymer*, **42**, 2785 (2001).
8. S. K. Shukla and M. A. Quraishi, *Appl. Poly. Sci*., **124**, 5130 (2012).
9. P. Manivel and S. Sathiyanarayanara, *Appl. Poly. Sci*., **110**, 2807 (2008).
10. H. Q. He, Y. J. Hou, L. He, J. Guo, C. H. Yang, W. Li, Y. X. Cai, J. J. Chen and Y. L. Hao, *Industry Water Treat*., **32**, 69 (2012).
11. J. G. Zhao, *Mater. Prot*., **41**(5), 23 (2008).
12. Y. Guo and S. Z. Song, *J. Chem. Industry Eng. (China)*, **51**, 788 (2000).
13. A. M. Atta, O. E. El-Azabawy, H. S. Ismail and M. A. Hegazy, *Corros. Sci*., **53**, 1680 (2011).
14. Y. H. Zhou, Y. N. Wang, H. Xie and Z. Q. Song, *Corros. Sci. Prot. Tech*., **15**, 324 (2003).
15. X. P. Qiu, J. Z. Chen, Q. Wang and Y. A. Liu, *Yunnan Chem. Tech*., **33**(5), 24 (2006).
16. S. Cheng, Y. S. Yin, S. G. Chen, X. T. Chang, L. N. Yan and T. Liu, *J. Chem. Indus. Engin*., **58**, 704 (2007).
17. L. Zhu, Y. F. Wang and B. X. Xu, *Corros. Prot*., **22**, 426 (2001) (in Chinese).
18. C. H. Yi, X. Q. Qiu, D. J. Yang and H. M. Lou, *J. Chem. Industry Eng. (China)*, **60**, 959 (2009).
19. X. J. Wang, X. F. Wang and S. W. Huang, *Mater. Prot*., **36**(12), 45 (2003).
20. H. Fu, X. H. Li, Y. X. Li and J. X. Liu, *J. Chin. Soc. Corros. Prot*., **31**, 265 (2011).
21. X. H. Li, H. Fu, Y. X. Li and N. Zhao, *Chin. J. Spectro. Labor*., **28**, 124 (2011).
22. X. H. Li, S. D. Deng and H. Fu, *Corros. Sci*., **62**, 163 (2012).
23. X. H. Li, S. D. Deng and H. Fu, *Corros. Sci*., **55**, 280 (2012).
24. R. Fuchs-Godec and V. Doleček, *Colloids Surf., A*, **244**, 73 (2004).
25. X. H. Li and S. D. Deng, *Corros. Sci*., **65**, 299 (2012).
26. F. Bentiss, M. Lebrini and M. Lagrenée, *Corros. Sci*., **47**, 2915 (2005).
27. E. Cano, J. L. Polo, A. La Iglesia and J. M. Bastidas, *Adsorption*, **10**, 219 (2004).
28. V. Branzoi, F. Branzoi and M. Baibarac, *Mater. Chem. Phys*., **65**, 288 (2000).
29. B. Ateya, B. El-Anadauli and F. El, *Corros. Sci*., **24**, 509 (1984).
30. G. Moretti, E. Guidi and F. Fabris, *Corros. Sci*., **76**, 206 (2013).
31. C. Cao, *Corros. Sci*., **38**, 2073 (1996).
32. C. N. Cao, Corrosion Electrochemistry Mechanism, Chemical Industrial Engineering Press, Beijing, 235 (2004), (in Chinese).
33. N. Labjar, M. Lebrini, F. Bentiss, N. E. Chihib, S. El Hajjaji and C. Jama, *Mater. Chem. Phys*., **119**, 330 (2010).
34. M. Lagrenée, B. Mernari, M. Bouanis, M. Traisnel and F. Bentiss, *Corros. Sci*., **44**, 573 (2002).
35. A. K. Singh and M. A. Quraishi, *Corros. Sci*., **52**, 152 (2010).
36. M. Lebrini, M. Lagrenée, H. Vezin, M. Traisnel and F. Bentiss, *Corros. Sci*., **49**, 2254 (2007).
37. Q. Qu, S.A. Jiang, W. Bai and L. Li, *Electrochim. Acta*, **52**, 6811 (2007).